

## Efficient Light Scattering from Nanochains Encapsulated in SnO<sub>2</sub> Hollow Spheres

Chunrong Ma<sup>1</sup>, Jinlin Lu<sup>2</sup>, Wei Shao<sup>3,\*</sup>, Feng Gu<sup>1</sup>, Shilong Jing<sup>1</sup>

<sup>1</sup> Key Laboratory for Ultrafine Materials of Ministry of Education, East China University of Science and Technology, Shanghai, 200237, China

<sup>2</sup> School of Materials and Metallurgy, University of Science and Technology Liaoning, Anshan, 114051, China

<sup>3</sup> Shanghai University, Shanghai, 200237, China

\*E-mail: [shaow@shu.edu.cn](mailto:shaow@shu.edu.cn).

Received: 11 January 2013 / Accepted: 4 February 2013 / Published: 1 March 2013

---

In this work, we demonstrated the synthesis of SnO<sub>2</sub> nanochains@hollow spheres homostructure by taking mesoporous silica microsphere (MS) as template. The filling degree of SnO<sub>2</sub> nanochain inside the hollow spheres could be easily tuned simply by tuning the structure and chain length of SnO<sub>2</sub> loaded within MS mesopores. The optimized SnO<sub>2</sub> nanochains@hollow spheres homostructure, when applied as the scattering layer in DSSCs, can remarkably increase the photocurrent of the cell due to the multiple light reflecting and scattering occurred in the unique hierarchical nanostructures. More significantly, the conversion efficiency possessed a 32.2% improvement compared to that derived from TiO<sub>2</sub> nanorod arrays.

---

**Keywords:** SnO<sub>2</sub> nanochains, SnO<sub>2</sub> hollow spheres, TiO<sub>2</sub> nanorod arrays, DSSCs

### 1. INTRODUCTION

Dye-sensitized solar cells (DSSCs) have attracted considerable attention since 11% photoconversion efficiency was reported derived from nanocrystalline TiO<sub>2</sub>[1,2]. Recently, intensive works on DSSC research have been focused on the design of TiO<sub>2</sub> photoanode films. However, it should be noted that the electron transfer mobility in TiO<sub>2</sub> ( $\sim 0.1\text{--}1.0\text{ cm}^2\text{V}^{-1}\cdot\text{S}^{-1}$ )[3] is not very good, lower than SnO<sub>2</sub> ( $\sim 100\text{--}200\text{ cm}^2\text{V}^{-1}\cdot\text{S}^{-1}$ )<sup>4</sup>. Moreover, SnO<sub>2</sub> possesses the larger band gap (3.6 eV)[5] than anatase TiO<sub>2</sub> (3.2 eV)[6], which can create fewer oxidative holes in the valence band. Therefore, SnO<sub>2</sub> has been considered as one of the promising alternative photoanode material for fabricating high efficiency DSSCs. However, compared with TiO<sub>2</sub>-based DSSCs, SnO<sub>2</sub>-based DSSCs suffered from the lower overall power conversion efficiency[7,8]. The low efficiency is in part related to the intrinsic

properties of SnO<sub>2</sub>. For example, a faster interfacial electron recombination and lower trapping density result from a 300 mV positive shift of the conduction-band edge of SnO<sub>2</sub> with respect to that of TiO<sub>2</sub>[9-11]. Recently, Qian et al. have reported the DSSCs' performance had a remarkable improvement by coating TiO<sub>2</sub> on SnO<sub>2</sub> hollow microspheres in the photoelectrode film[12], which could not only enhance the light scattering, but also facilitate the electron transport. Furthermore, multishelled hierarchical structures have also been developed and exhibited intriguing light scattering using as light scattering layer. Dong et al. reported that the preparation of multishelled ZnO hollow microspheres showed greatly enhanced solar conversion efficiency due to the enhancement of light scattering and reflecting[13]. Very recently, our group has synthesized the multishelled TiO<sub>2</sub> nanoplates, which demonstrated improved cell performance from 5.27 to 6.53% due to the enhanced light harvesting capability[14].

To further improve the SnO<sub>2</sub>-based DSSCs efficiency, hence, the novel SnO<sub>2</sub> nanochains@hollow spheres were designed and synthesized by taking MS as the templates, the 3D SnO<sub>2</sub> nanochains were encapsulated inside the hollow microsphere. By tuning the length of SnO<sub>2</sub> nanochains, the filling degree of SnO<sub>2</sub> nanochains inside the hollow spheres could be tuned. Due to the multiple light reflecting and scattering occurred in the hierarchical structures, the nanochains@hollow spheres-derived DSSCs improved the cell performance.

## 2. EXPERIMENTAL

### 2.1 Formation of SnO<sub>2</sub> nanochain@hollow spheres

SnO<sub>2</sub>-nanochain-loaded MS as well as the remodeled MS microspheres have been reported by our group previously[15]. Firstly, the loading of SnO<sub>2</sub> nanocrystallites inside the channels of MS (MS/SnO<sub>2</sub>) were prepared by hydrothermal method in our previous work. The second step was to coat SnO<sub>2</sub> nanocrystallites onto the MS/SnO<sub>2</sub>. 0.06 g-0.18 g of MS/SnO<sub>2</sub> was dispersed in 30 ml of ethanol/water mixture (37.5 % ethanol vol %) by ultrasonication. 0.90 g of urea and 0.10 g of potassium stannate trihydrate were added to the mixture by vigorous stirring. Then, the turbid suspension was transferred into 40 ml Teflon-lined stainless-steel autoclave, which was then heated at 170 °C for 24 h in an airflow electric oven. After the autoclave was cooled to room temperature, the white products were harvested by centrifugation and washed with deionized water and ethanol before drying at 80 °C overnight. The silica cores were etched by the dilute ethanol/water solution of HF ( ~ 2 %).

Preparation of SnO<sub>2</sub>/TiO<sub>2</sub> Heterogeneous Composite Films. In the fabrication of DSSCs, the TiO<sub>2</sub> nanoroad arrays were first synthesized onto F-doped SnO<sub>2</sub> conducting glass (FTO, Nippon Sheet Glass, SnO<sub>2</sub> :F, 15 ohm/sq). 10 ml toluene mixed with 1ml tetrabutyl titanate. After 10 min stirring, 1 ml titanium tetrachloride (1 M in toluene) and 1 ml hydrochloric acid (37 wt %) were added. After another 30 min stirring, the mixture was transferred into a 50 ml Teflon-lined autoclave, and the clean FTO substrate was placed at an angle against the wall of the autoclave with the conducting side facing down. The hydrothermal synthesis was maintained at 150 ~ 180 °C for 3 h ~ 5 h, the autoclave was

cooled to room temperature. The products were rinsed with deionized water and dried at 80 °C for 60 min.

1.00 g of the prepared nanochains@hollow spheres was dispersed in 1.00 ml of terpineol (Sigma-Aldrich). After being ground for 20 min, 0.025 g of ethyl cellulose (EC; M70, Sinopharm) and 0.40 ml Triton X-100 (Sinopharm, cp) were introduced and ground for 30 min. Subsequently, 4.00 ml of terpineol was added, and the mixture was ground for another 30 min. Finally, to obtain the double layer film, the resulting colloidal suspension was deposited on TiO<sub>2</sub> nanorods arrays with an active area of 0.25 cm<sup>2</sup> by the screen-printing technique. The heterogeneous composite films were annealed at 450 °C for 30 min in air. For photosensitization studies, the heterogeneous composite films were immersed in anhydrous ethanol solution containing 0.50 mM of Ru dye ((Bu<sub>4</sub>N)<sub>2</sub>[Ru(Hdcbpy)<sub>2</sub>-(NCS)<sub>2</sub>], known as N719, Solaronix) for 24 h at room temperature. Pt counter electrode was prepared on the transparent conducting glass using 0.70 mM of H<sub>2</sub>PtCl<sub>6</sub> solution, it was subsequently annealed at 380 °C for 20 min in air. The redox electrolyte consisted of 0.60 M of BMII (1-butyl-3-methylimidazoliumiodide), 0.03 M of I<sub>2</sub>, 0.10 M of guanidinium thiocyanate, and 0.50 M of 4-tert-butylpyridine in a mixture of acetonitrile and valeronitrile (volume ratio, 85:15). The two electrodes were sealed together with the hot-melt polymer film.

## 2.2 Characterization

The general morphology and crystallinity of the samples were examined by scanning electron microscopy (SEM; Hitachi S-4800), transmission electron microscope (TEM-2100), and high-resolution transmission electron microscope (HRTEM; JEM-2010). The X-ray diffraction (XRD) patterns of the samples were measured by using a Japan Rigaku D/max 2550 VB/PC diffractometer with Cu K $\alpha$  radiation ( $\lambda=0.15418$  nm). The band gap energy of SnO<sub>2</sub> powders and absorbance spectra with dye-covered heterogeneous composite films were obtained using a scan UV-vis-NIR spectrophotometer (Varian, Cary 500) equipped with an integrating sphere assembly. The incident monochromatic photons to current conversion efficiency (IPCE) spectra were measured using an Oriel 300 W xenon arc lamp and a lock-in amplifier M 70104 (Oriel) under monochromator illumination, which was calibrated with a monocrystalline silicon diode.

## 3. RESULTS AND DISCUSSION

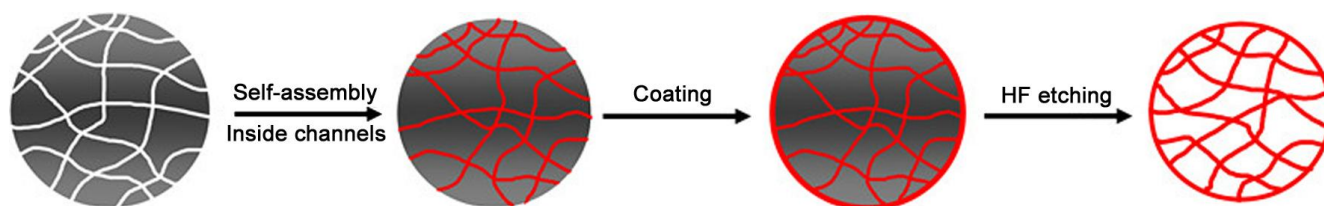


**Figure 1.** Schematic illustration of the formation of the SnO<sub>2</sub> nanochains@hollow spheres.

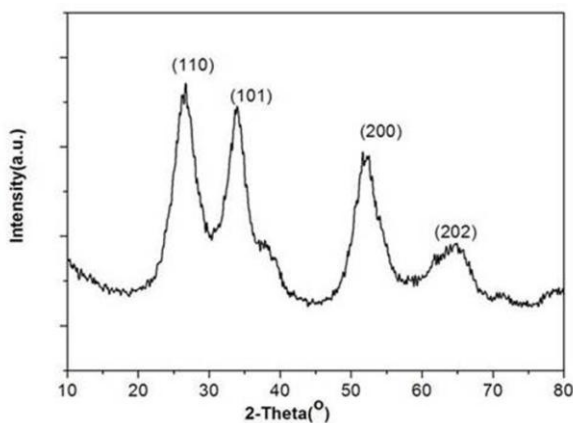


**Figure 2.** XRD pattern of SnO<sub>2</sub> nanochains@hollow spheres.

The SnO<sub>2</sub> nanochains@hollow spheres were prepared by the hydrothermal method using MS spheres as template. Figure 1 shows the formation process of the SnO<sub>2</sub> nanochains@hollow spheres. Firstly, the SnO<sub>2</sub> nanocrystals underwent self-assembly inside the channels of the MS template spheres. Because of enriched with Si-OH groups on the surface of MS, the numerous SnO<sub>2</sub> nuclei with positively charges can attach to the negatively charged inner surface of MS. The formation process of SnO<sub>2</sub> nanocrystallites in the MS channels can be summarized as follows:



After the primary seed-incubation stage, the seeds intend to grow bigger until they finally became stable. And then the SnO<sub>2</sub> coating was deposited on the surface of SnO<sub>2</sub>/MS spheres via the second hydrothermal method.

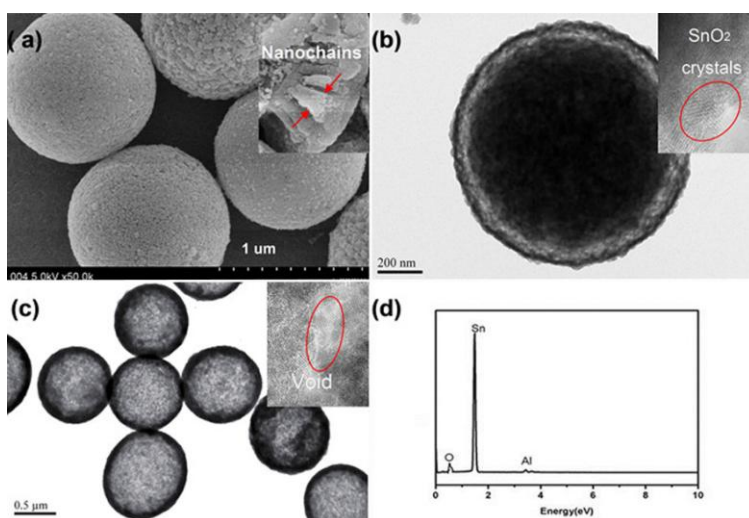


**Figure 3.** (a, b) SEM and TEM images of nanochains@hollow spheres before etching MS. (c, d) TEM and EDS results of SnO<sub>2</sub> nanochains@hollow spheres.

Finally, the SnO<sub>2</sub> nanochains@hollow spheres were obtained after removing the MS template spheres with HF solution for 24 h. Figure 2 shows the XRD pattern of the as-prepared SnO<sub>2</sub> nanochains@hollow spheres. Several peaks were distinctly recorded to be centered at 26.5°, 33.6°, 37.8° and 69.9°, respectively. All the identified peaks can be assigned to tetragonal rutile SnO<sub>2</sub> (JCPDS NO. 41-445). The presence of broad peaks indicates the SnO<sub>2</sub> has a very small crystalline size.

From the field-emission scanning electron microscopy (FESEM) image shown in Figure 3a, uniform spheres with a diameter of ~ 1 μm can be obtained. The surface is rough, indicating the successful deposition of SnO<sub>2</sub> nanocrystallites on the surface of the SnO<sub>2</sub>/MS spheres. The inset of Figure 3a shows a randomly broken sphere of the MS/SnO<sub>2</sub>@hollow spheres. The shell thickness found to be about 50 nm. SnO<sub>2</sub> nanocrystallites-aggregated SnO<sub>2</sub> nanochains can also be observed in the cavity. The formation of SnO<sub>2</sub> nanochains is attributed to the confinement of the channels in the MS spheres, which was reported in our previous work[15]. Figure 3b and 3c show the TEM images of the SnO<sub>2</sub> nanochains@hollow spheres before and after removing the MS templates. The outer SnO<sub>2</sub> shell is about 50 nm in thickness, consistent with the FESEM results. Furthermore, the enlarged TEM image in the inset of Figure 3b indicates that the SnO<sub>2</sub> shell is constructed by ultrafine crystallites, which is in agreement with the corresponding XRD results. From the HRTEM image shown in the inset of Figure 3c, a three-dimension (3D) network of SnO<sub>2</sub> nanochains can be found in the cavity of the SnO<sub>2</sub> nanochains@hollow spheres after removing the silica core. Furthermore, the atomic ratio of Sn to O is estimated to 0.5 from EDS spectrum shown in Figure 3d, and only minor SiO<sub>2</sub> can be detected. The unique SnO<sub>2</sub> hierarchical structure, combining the inside 3D-network SnO<sub>2</sub> nanochains core and outer SnO<sub>2</sub> nanocrystallites shell, would improve cell performance when used the novel scattering layer in DSSCs, due to the enhanced light harvesting capability.

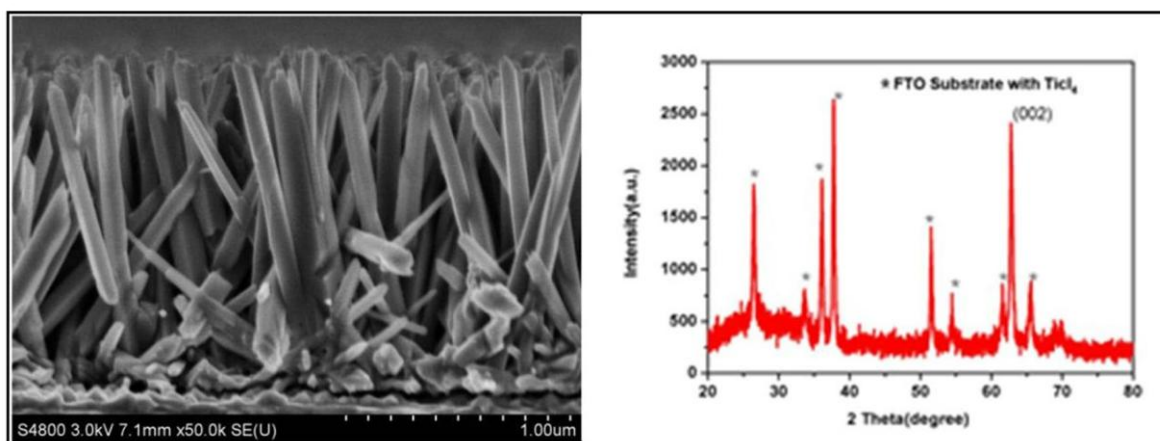


**Figure 4.** cross-sectional FESEM image and XRD of the vertically oriented self-organized TiO<sub>2</sub> nanowire array grown on FTO

Light scattering properties have been generally accepted as one important attribute in determining light harvesting efficiencies. The traditional photoelectrode architecture is a several micron-thick film composed of nanocrystalline TiO<sub>2</sub> nanoparticles on transparent substrate. However, the electron diffusion coefficient of these nanoparticulate films is several orders of magnitude smaller

than the value in bulk single-crystal  $\text{TiO}_2$ , due to electron traps at the contacts between nanoparticles[16-18]. Herein, the bilayer photoanode was screen-printed with the scattering nanochains@hollow spheres layer and the  $\text{TiO}_2$  nanorods arrays bottom layer as the single-crystalline  $\text{TiO}_2$  nanorods arrays films monstrate lower recombination and excellent electron transmission. In this work, rutile  $\text{TiO}_2$  nanorods arrays with 90 nm in diameter and 1.4  $\mu\text{m}$  in thickness(as shown in Fig 4) prepared by hydrothermal method[19] were used as the bottom layer in the photoelectrode. And the prepared nanochains@hollow spheres were taken as the scattering layer. After fabricating the photoelectrode film, the length of  $\text{SnO}_2$  nanochains inside the hollow spheres has been found a remarkable influence on the light scattering as well as the cell efficiency.

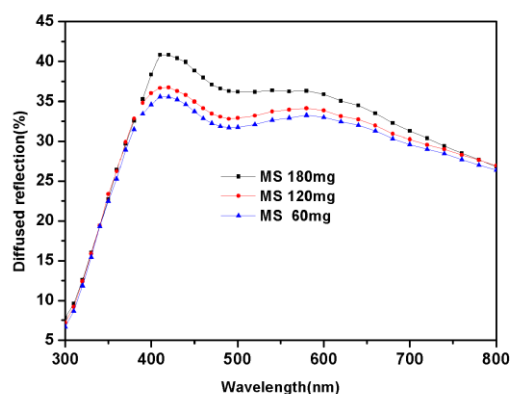


**Figure 5.** UV-Vis diffused reflection spectra of undyed films derived from different  $\text{SnO}_2$  nanochains length.

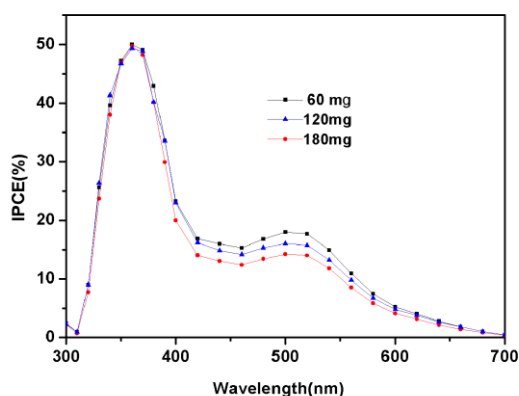


**Figure 6.** IPCE spectra of the cells based on the photoelectrode films derived from different  $\text{SnO}_2$  nanochain length.

To better understand the influence of the  $\text{SnO}_2$  nanochain on light scattering, the structure and length of the nanochains have been tuned by adjusting the amount of MS used when loading  $\text{SnO}_2$  nanocrystallites inside the channels of the MS.  $\text{SnO}_2$  crystallites changed gradually from separated particles to chains inside the channels with MS amount decreasing. Short chains can be formed when

180 mg MS were used. Less MS amount (e.g., 120 mg), longer SnO<sub>2</sub> chains would be formed. Furthermore, if much less MS was used (e.g., 60 mg), good SnO<sub>2</sub> network can be formed. Based on our previous study, the SnO<sub>2</sub> nanochains are in fact composed of nanocrystals with size of ~ 2 nm that are attached with each other in series. The quantity of SnO<sub>2</sub> nuclei formed at the beginning is discrepant according the concentration of MS precursor with the formation of SnO<sub>2</sub> nanocrystals with strong tensile strain. With reaction proceeding, the SnO<sub>2</sub> nanoparticles grew bigger until they were blocked by the sidewalls of the channel. They were confined in the channel and cannot grow. When using smaller amounts of MS with the other experimental conditions unchanged, that is less SnO<sub>2</sub> nuclei formed inside the channels, the reaction system would supply sufficient precursor for the nuclei to form bigger crystallites, and as a result the attached to each other randomly to form chains. As the reaction proceeded, rearrangement and welding of the attached dots took place with strain relaxation, a quasi-oriented attachment would be realized. Figure 5 shows the diffused reflection spectra of the undyed bilayer films. The reflectance of bilayer films is found to be markedly higher with increasing SnO<sub>2</sub> nanochains length over the entire region, indicating a superior light scattering effect. After forming the SnO<sub>2</sub> network inside the hollow spheres, better reflection can be obtained due to the confinement of incident light within the nanochains@hollow spheres. Figure 6 shows the photoelectron conversion efficiency (IPCE) spectra of the fabricated solar cells, the IPCE values become higher with increasing SnO<sub>2</sub> nanochain length at the maximum value at 525 nm. The improvement can be attributed to the enhanced electron injection and charge-transfer efficiency as well as to the higher amount of dye absorption.

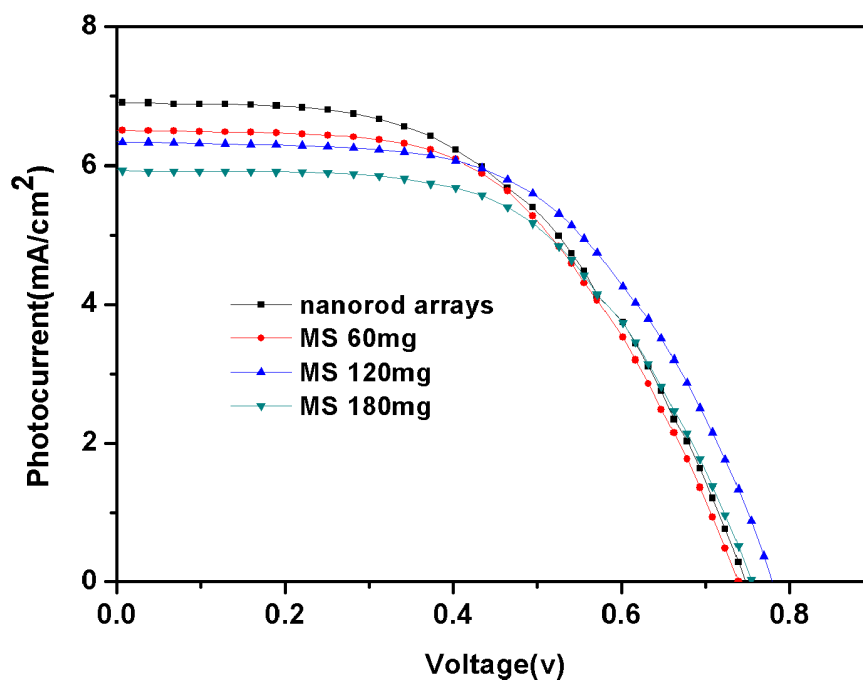


**Figure 7.** I–V characteristics of DSSCs with the photoelectrode films derived from different SnO<sub>2</sub> nanochain length.

**Table 1.** Summarized Cell Performance of the Fabricated DSSCs

Cell	DSSC from	$V_{oc}/V$	$J_{sc}/\text{mA}/\text{cm}^2$	FF/%	$\eta/\%$	AbsorbedDye ( $\times 10^{-7}$ mol $\cdot$ cm $^{-2,a}$ )
1	TiO <sub>2</sub> rod array	0.73	5.89	61.09	1.71	0.73
2	MS 180 mg	0.78	6.23	58.70	2.09	1.03
3	MS 120 mg	0.73	6.48	58.60	2.12	1.10
4	MS 60 mg	0.72	6.93	53.33	2.26	1.13

<sup>a</sup> Dye-adsorbed films with a dimension of 0.25 cm<sup>2</sup> were used for estimating the adsorbed dye concentration.

The characteristic current (I)–voltage (V) curves of the fabricated DSSCs are given in Figure 7. It can be seen that both the short-circuit current density ( $J_{sc}$ ) and conversion efficiency ( $\eta$ ) of the cell increase with the length of SnO<sub>2</sub> nanochains inside the hollow spheres (Table 1). This enhanced photocurrent could be attributed to increased active surface area and enable multiple light reflecting and scattering among the nanochain network. The cell derived from the SnO<sub>2</sub> nanochains@hollow spheres with 60mg-MS used possesses a  $J_{sc}$  of 6.93 mA/cm<sup>2</sup> and overall  $\eta$  of 2.26%. The conversion efficiency is 32.2% higher than that derived from TiO<sub>2</sub> nanorod arrays ( $\eta=1.71\%$ ), due to increased light absorption by the beneficial multi-layered spherical structure. The multiple nanochains inside the nanosphere can not only multireflect, but also scatter the incident light of different wavelengths in the range of visible light. Both the factors contribute to make an improvement of  $J_{sc}$ .

#### 4. CONCLUSION

In summary, SnO<sub>2</sub> nanochains were successfully encapsulated inside hollow spheres with variable nanochain length by taking mesoporous silica microsphere (MS) as template. After loading SnO<sub>2</sub> nanochains within the MS mesopores, a hydrothermal method was employed to coat a polycrystalline SnO<sub>2</sub> layer on the surface of SnO<sub>2</sub>-loaded MS to form the special core/shell heterostructure. After removing the silica core, nanochain-encapsulated SnO<sub>2</sub> hollow spheres would be obtained. By tuning the structure and chain length of SnO<sub>2</sub> loaded within MS mesopores, the filling degree of SnO<sub>2</sub> nanochain inside the hollow spheres could be tuned. When applied as the scattering layer in DSSCs, the photocurrent of the cell increased remarkably with nanochain length due to the multiple light reflecting and scattering occurred in the hierarchical structures. The results indicated a 32.2% improvement in comparison with that derived from TiO<sub>2</sub> nanorod arrays.

#### ACKNOWLEDGMENT

This work was supported by the National Natural Science Foundation of China (20925621, 21176068, 21106038, 21136006, 51203093).

## References

1. U. M. K. Shahed, M. Al-Shahry, B. William and Jr. Ingler, *Science*, 297 (2002) 2243
2. M. Grätzel and J. Photochem. Photobiol, *Chem.*, 164 (2004) 3
3. R. G. Breckenridge and W. R. Hosler, *Phys Rev.*, 91 (1953) 793
4. C. G. Fonstad and R. H. J. Rediker, *Phys Rev.*, 42 (1971) 2911
5. E. E. Kohnke, *J. Phys. Chem. Solids*, 36 (1965) 3931
6. L. Amy, Q. Lu. Guang, T. John and Jr. Yates, *Chem Rev.*, 95 (1995) 735
7. S. Chappel , A. Zaban, Nanoporous, *Sol. Energy Mater. Sol. Cells*, 71 (2002) 141
8. A. Usami, *Chem. Phy. Lett.*, 84 (2004) 3397
9. W. Shao, F. Gu, C. Z. Li and M. Lu, *Ind. Eng. Chem. Res.*, 49 (2010) 5453
10. P.V. Kamat, I. Bedja, S. L. Hotchandani and K. J. Patterson, *Phy.Chem*, 100 (1996) 4900
11. R. Yue, Sh. Chen, B. Lu, C. Liu and J. Xu, *J Solid State Electrochem*, 10 (2011) 539
12. J. F. Qian, P. Liu, Y. Xiao, Y. Jiang, Y. L. Cao, X. P. Ai and H. X. Yang, *Adv. Mater.*, 21 (2009) 3663
13. Z. H. Dong, X. Y. Lai, J. E. Halpert, N. L. Yang, L. X. Yi, J. Zhai, D. Wang, Z. Y. Tang and L. Jiang, *Adv.Mater.*, 24 (2012) 1046
14. W. Shao, F. Gu, L. L. Gai and C. Z. Li, *Chem.Commun.*, 47 (2011) 5046
15. F. Gu, X. Ren, J. Zhang, W. Shao and C. Z. Li, *Ind. Eng. Chem. Res.*, 50 (2011) 12542
16. P. Wang, Y. Zhu, X. Yang, C.Z. Li and H. L. Du, *Acta. Mater.*, 56 (2008) 1144
17. A. Solbrand, H. Lindstrom, H. Rensmo, A. Hagfeldt, S. E. Lindquist and S. Sodergren, *J. Phys. Chem. B*, 101 (1997) 2514
18. J. Van de Lagemaat, N. G. Park, *J. Frank, J. Phys. Chem. B*, 104 (2000) 2044
19. B. Liu, E. S. Aydil, *J. Phys. Chem. Solids*, 131 (2009) 3985